Catalysis Today 173 (2011) 44–52

Contents lists available at ScienceDirect

Catalysis Today

journal homepage: www.elsevier.com/locate/cattod

Catalytic performances of large pore Ti-SBA15 supported Pt nanocomposites for the citral hydrogenation reaction

Tchirioua Ekou[a,b], Catherine Especel[a,*], Sébastien Royer[a]

[a] LACCO, UMR 6503 CNRS, 40 Avenue du Recteur Pineau, 86022 Poitiers Cedex, France
[b] Laboratoire de Thermodynamique et de Physico-Chimie du Milieu, Université d'Abobo-Adjamé, 02 Bp 801 Abidjan 02, Cote d'Ivoire

ARTICLE INFO

Article history:
Received 7 December 2010
Received in revised form 22 March 2011
Accepted 11 May 2011
Available online 21 June 2011

Keywords:
Pt
Titania
Silica
Mesoporous materials
Nanoparticles
Citral hydrogenation
SMSI effect

ABSTRACT

Pt/*x*%Ti-SBA15 catalysts (*x* corresponding to the wt.% TiO_2 loading in the Ti–SiO_2 composite, in the range 25–60%) were synthesized by titanium precursor grafting in preformed mesoporous silica. Materials were characterized by several techniques, including elemental analysis, XRD, TEM and N_2-sorption isotherms to achieve structural and textural properties description. Different pore sizes were obtained for the SBA-15 materials, by using or not hexane as swelling agent. The catalytic performances of these original materials were evaluated for the selective hydrogenation of citral (α,β-unsaturated aldehyde), and compared with those of Pt/SBA and Pt/TiO_2 P25 reference catalysts. Pt/*x*%Ti-SBA15 catalysts present high specific surface, with TiO_2 nanoparticles and Pt^0 clusters located inside the hexagonal mesopore structure of silica. During citral hydrogenation, the selectivity towards unsaturated alcohols (nerol and geraniol) varies as a function of the support nature as follows: Pt/*x*%Ti-SBA15 > Pt/TiO_2 P25 ≫ Pt/SBA. The results are discussed in term of variable metal-support interaction (SMSI) generated by the partial reduction of TiO_2 species, this SMSI effect being reported more important over anatase TiO_2 nanoparticles dispersed inside the mesostructure than over large crystals encountered in the classical P25 support.

1. Introduction

Silica materials with hexagonal structured mesopore network, as developed in SBA-15 materials, have been extensively studied since the first reports dealing with their synthesis using various templating agent [1,2]. Their high specific surface area, large pore volume and adjustable pore size (in the range from a few nanometer to more than 20 nm) make them ideal supports for the preparation of highly dispersed heterogeneous catalysts, while the controlled pore structure is a great advantage for the identification of the textural parameter effect on the catalytic properties [3–6]. The SBA silica family has been intensively modified to generate active materials for heterogeneous catalysis. Thus, the introduction of different atoms such as Al, Ti and Zr into organized mesoporous siliceous structures was already studied [7,8]. Various synthesis routes such as titania precursor impregnation/grafting [9–12], titanium atom incorporation by direct synthesis in the silica framework [13], or incorporation of preformed titania nanoparticles before silica condensation [14] are reported as efficient routes to generate dispersed titanium species. We can also note that mesostructuration of bulk titania was also studied, but leads to materials having very limited thermal stability, avoiding their use as catalytic support for high temperature reactions.

Moreover, titania has attracted much attention during the past 30 years due to the strong metal-support interaction (SMSI) occurring on the surface of TiO_2 supported materials, and allowing tuning of both catalytic activities and selectivities for various reactions including selective hydrogenation and dehydrogenation [15–19]. Thanks to its reducible surface properties, titania was often used as model support [20–22], and consequently SMSI effect over the titania-noble metal systems was studied extensively [15,16,23–27].

The present study focuses on the preparation of Pt-based catalysts supported on TiO_2-modified mesostructured silica for liquid phase hydrogenation of citral. Citral is a α,β-unsaturated aldehyde (3,7-dimethyl-2,6-octadien-1-al) produced essentially from the oil extracted from lemon. The valorization of this compound can occur by the selective hydrogenation of the carbonyl function, leading to unsaturated alcohol (geraniol/nerol) largely used by the perfume industry (soaps, detergents. . .). Monometallic catalysts containing noble metal like Pt supported on conventional oxides, such as SiO_2, are active for the hydrogenation of the ethylenic C=C double bond but very few active for the hydrogenation of the C=O carbonyl function, given rise to poor selectivity in valuable molecules. In order to improve the unsaturated alcohol selectivity, we recently studied monometallic catalysts modified either by support effects (SMSI effect induced by reducible support such as TiO_2) or by addition of a second metal (Sn, Ge) [28,29]. In this work, nanocom-

* Corresponding author. Tel.: +33 0 5 49 45 39 94; fax: +33 0 5 49 45 37 41.
E-mail address: catherine.especel@univ-poitiers.fr (C. Especel).

0920-5861/$ – see front matter © 2011 Elsevier B.V. All rights reserved.
doi:10.1016/j.cattod.2011.05.016

posites Pt/*x*%Ti-SBA samples (*x* ranging from 25 to 60 wt.%) were synthesized by post-grafting of titanium organic precursor over preformed SBA-15 type silica support to achieve, after thermal stabilization, titania nanodomains dispersed and accessible in the silica porosity. All composites were fully characterized using conventional techniques. Afterwards, the liquid phase hydrogenation of citral was performed at 70 °C under hydrogen pressure (7 MPa) in order to compare the catalytic performances of the Pt/*x*%Ti-SBA samples with those of the Pt supported on bulk TiO_2 P25 catalyst.

2. Experimental

2.1. Preparation of Pt-based mesoporous catalysts

All chemicals were used as received. Poly(ethylene glycol)-*b*-poly(propylene glycol)-*b*-poly(ethylene glycol) $EO_{20}PO_{70}EO_{20}$ (Pluronic P123), titanium (IV) isopropoxide ($Ti(O^iPr)_4$, 97%) and hydrochloric acid (HCl, 37 wt.%) were purchased from Aldrich. Tetraethyl orthosilicate (TEOS, ≥99%) was purchased from Fluka. Anhydrous ethanol (>99.9%) was purchased from Merck.

The SBA-15 mesoporous material, presenting a 8 nm pore diameter, was prepared using classical synthesis conditions [30] and was detailed in previous articles [11,12]. Hydrothermal treatment was performed at 140 °C in order to achieve large pore size and limited microporosity. In order to obtain larger pore size (~20 nm), hexane was used as swelling agent. The synthesis of the 20 nm pore size SBA-15 type silica is prepared under the following synthesis composition 1 TEOS: 0.0168 P123: 4.02 C_6H_{14}: 0.0295 NH_4F: 4.42 HCl: 186 H_2O (mole fraction). The solution was maintained at room temperature for 24 h under stirring for aging. The milky solution is thereafter transferred into a Teflon-lined autoclave, and heated at 140 °C for 48 h. Silica was recovered by filtration. Before use and characterization, the two supports (8 nm and 20 nm) were calcined under air at 550 °C for 4 h (temperature increase rate = 1 °C min^{-1}).

In all cases, the freshly calcined SBA-15 support (8 nm or 20 nm pore size) and titanium isopropoxide ($Ti(O^iPr)_4$) as titanium source were used. Sample preparation consisted in the slow impregnation of a dilute solution of $Ti(O^iPr)_4$ in dry ethanol (volume ratio $V_{Ti(O^iPr)_4}/V_{EtOH} = 0.05$, impregnation at 20 °C). Titania loading was adjusted at 25 wt.%, 40 wt.% or 60 wt.% of TiO_2 in the final material after calcination at 400 °C (temperature increase rate = 1 °C min^{-1}).

1.5 wt.% of platinum was finally impregnated using a hexachloroplatinic acid solution (H_2PtCl_6). After impregnation, the solids were calcined at 400 °C (temperature increase rate = 10 °C min^{-1}), then reduced under hydrogen flowing at 300 °C for 4 h. A 1.5 wt.% Pt/TiO_2 P25 reference catalyst (P25 titania from Degussa) was prepared for comparison and activated under the same conditions.

2.2. Catalysts characterization

Elemental analysis (platinum, titanium and silicon) was performed using a sequential scanning inductively coupled plasma optical emission spectrometer (ICP-OES), Perkin. Samples were dissolved in HF solution under microwave heating before analysis.

Specific surface area, pore size distribution and pore volume were obtained from N_2-sorption isotherms collected on a TRISTAR instrument from Micromeritics. Samples were degassed for 1 night at 300 °C until residual pressure in the analysis cell was below 0.15 mbar. The specific surface area, S_{BET}, was determined from the linear part of the BET plot. The mesopore size distribution was determined by the non local density functional theory (NLDFT) method and calculated using the Autosorb-1 1.52 software. The kernel selected was N_2 on silica assuming cylindrical pore geometry and the equilibrium based on the desorption branch. Pore volume is determined on the isotherms at $P/P_0 = 0.97$.

Powder X-ray diffraction (XRD) patterns were collected on a Bruker AXS D5005 X-ray diffractometer, using a CuKα radiation (λ = 1.54184 Å) as X-ray source. The signal was recorded for 2θ comprised between 0.75° and 3° with a step of 0.01° (step time of 10 s) and for 2θ comprised between 10° and 75° with a step of 0.05° (step time of 2 s). Phase identification was made by comparison with JCPDS database.

Transmission electron microscopy (TEM) was performed on a JEOL 2100 UHR instrument (operated at 200 kV with a LaB_6 source and equipped with a Gatan Ultra scan camera). All the samples were embedded in a polymeric resin (spurr) and cut into sections as small as 50 nm with an ultramicrotome equipped with a diamond knife. Cuts were then deposited on a Cu grid holey carbon film. Average particle sizes were determined by measuring at least 100 particles for each sample analyzed, from at least 5 different micrographs.

2.3. Citral hydrogenation

The liquid phase hydrogenation of citral was carried out in a 300 mL stirred autoclave (Autoclave Engineers, fitted with a system for liquid sampling) at 70 °C and at constant pressure of 7 MPa. Pre-reduced catalysts (400 mg) were immersed into 90 mL of solvent (isopropanol 99%) without exposure to air before introduction into the autoclave. After a first flush with nitrogen and a second with hydrogen, the temperature was raised to 70 °C under 3 MPa of hydrogen. Then a mixture of substrate (3 mL of citral) and of solvent (10 mL) was loaded into the autoclave through a cylinder under a 7 MPa hydrogen pressure. The introduction of the citral solution corresponds to the beginning of the reaction, and stirring was switched on. Liquid samples were analyzed by gas chromatography on a Thermofinnigan chromatograph equipped with a FID detector and a capillary column DB-WAX (J&W, 30 m, 0.53 mm i.d.) using nitrogen as carrier gas.

3. Results and discussion

3.1. Characterization of the catalysts

1.5 wt.% Pt/*x*%Ti-SBA samples were prepared using different amounts of Ti-isopropoxide in order to obtain *x* wt.% TiO_2 in the final material (*x* = 25, 40 or 60). These samples will be denoted as Pt/*x*%Ti-SBA*y*nm, where *y* represents the initial pore size of silica SBA-15 prepared. All the catalysts are listed in Table 1 with their name, elemental composition and main physical and structural characteristics. The 1.5 wt.% Pt/TiO_2 P25 reference catalyst is also prepared for comparison.

3.1.1. X-ray diffraction

Powder X-ray diffraction (XRD) was used to assess the structural ordering of the parent silica SBA, and of the Ti-SBA and Pt/Ti-SBA materials for both 8 and 20 nm pore sizes. For each catalyst prepared on the SBA8 nm support, the small angle X-ray diffractograms are well resolved and present the three characteristic peaks corresponding to reflections on the (1 0 0), (1 1 0) and (2 0 0) planes of a 2D hexagonal structure for silica SBA-15 (Fig. 1A). The more intense peak near 2θ values of ca. 0.95° is assigned to the (1 0 0) reflection due to the long-range ordering of the SBA hexagonal pore structure [31]. Incorporation of Ti and Pt does not affect the structure of the materials, since no noticeable modification of the small angle X-ray diffraction patterns is observed, and all the reflection intensities are still in agreement with those of the structure of pure SBA-15. The presence of the peak $2\theta = 0.95°$ is obvious for each sample and so implies that the ordered hexagonal pore structure is maintained throughout the grafting/impregnation–drying–calcination

Table 1
Physical properties of 1.5 wt.% Pt/*x*%Ti-SBA15 catalysts.

Pt/Support	TiO_2 (wt.%)	Pt (wt.%)	S_{BET} ($m^2\ g^{-1}$)	D_p (nm)	V_p ($cm^3\ g^{-1}$)	D_{Ti}[a]$_{crystal}$ (nm)	D_{Pt} (nm)	Phase
Pt/SBA8 nm	0	1.6	390	8.0	0.80	–	1.3	–
Pt/25%Ti-SBA8 nm	25	1.5	383	6.0	0.62	4.1	0.9–1.4	Anatase
Pt/40%Ti-SBA8 nm	40	1.5	346	5.1	0.48	4.6	0.9–1.4	Anatase
Pt/SBA20 nm	0	1.6	342	19.1	1.97	–	0.9–1.4	–
Pt/25%Ti-SBA20 nm	25	1.5	340	16.8	1.02	4.9	0.9–1.4	Anatase
Pt/40%Ti-SBA20 nm	40	1.7	339	12.6	1.06	5.3	0.9–1.4	Anatase
Pt/60%Ti-SBA20 nm	60	1.6	279	8.0	0.65	6.6*	0.9–1.4	Anatase
Pt/TiO_2 P25	100	1.4	49	8.0	–	–	2.1	Anatase/rutile (75/25)

[a] Evaluated using TEM or Scherrer equation from the X-ray line broadening (*).

and reduction process. For the 20 nm pore size support (SBA20 nm), the large increase in cell parameter and consequently the important decrease in 2θ values of the pore structure reflection unfortunately avoid the use of this technique to characterize the structure of this support.

Wide angle powder XRD measurements were performed to investigate the presence of any crystalline species in the materials. The diffraction patterns for all catalysts *x*%Ti-SBA8 nm and *x*%Ti-SBA20 nm composites (Figs. 1B and Fig. 2) were similar to this of the initial support, with a single broad peak centered at 23° characteristic of amorphous silica. Notably, no peak characteristic of an anatase structure, associated with the formation of a crystallized TiO_2 phase can be detected at low titanium loading (25 wt.%), indicating that the grafting of titanium does not lead to the formation of a titania phase organized on a large scale, and results in the formation of small TiO_2 particles as already observed in our previous works [11,12]. On the other hand, the presence of TiO_2 anatase structure is observed on the XRD pattern since 40 wt.%. The growth of anatase nanoparticles with the increase of the amount of Ti(O^iPr)$_4$ precursor can be explained by the number of Ti species dispersed in the support surface. Indeed, small amounts of Ti species will easily graft on the silica surface, and the probability to aggregate remains low. In contrast, higher Ti concentration in the deposition sol causes the formation of larger TiO_2 clusters, due to the limited silica sites for grafting. Luan and Kevan [32] have also studied the impregnation of titanium into mesoporous SBA-15 via incipient-wetness impregnation. They observed that titanium is monoatomically dispersed on SBA-15 silica wall surface at low content, while a TiO_2 anatase film forms if TiO_2 loading is high. The calcination of a film at high temperature (as in our case, 400 °C) can result in its cracking when anatase crystallizes. The platinum deposition and reduction steps also result in important modifications of the material structural properties. Indeed, the anatase crystalline phase is easily detected by XRD whatever the support (8 nm or 20 nm) or the titania loading (Figs. 1B and Fig. 2). The average crystal size of TiO_2 particles calculated using the Scherrer equation (or by statistical analysis on TEM micrographs when anatase reflections are not enough defined) are given in Table 1. The titania crystal size remains limited for all Pt-based catalysts (between 4.1 and 6.6 nm), and remains below the pore size of the silica support, which suggests a satisfying dispersion of the nanoparticles in the porosity. Metallic platinum reflections are however not detected, excepted when Pt is dispersed on pure silica (Pt/SBA8 nm and Pt/SBA20 nm, indicated by a "*" in Figs. 1B and Fig. 2). Such a result is consistent with a high dispersion of the metallic phase in the Ti-containing materials, while Pt is probably slightly less dispersed when supported on silica.

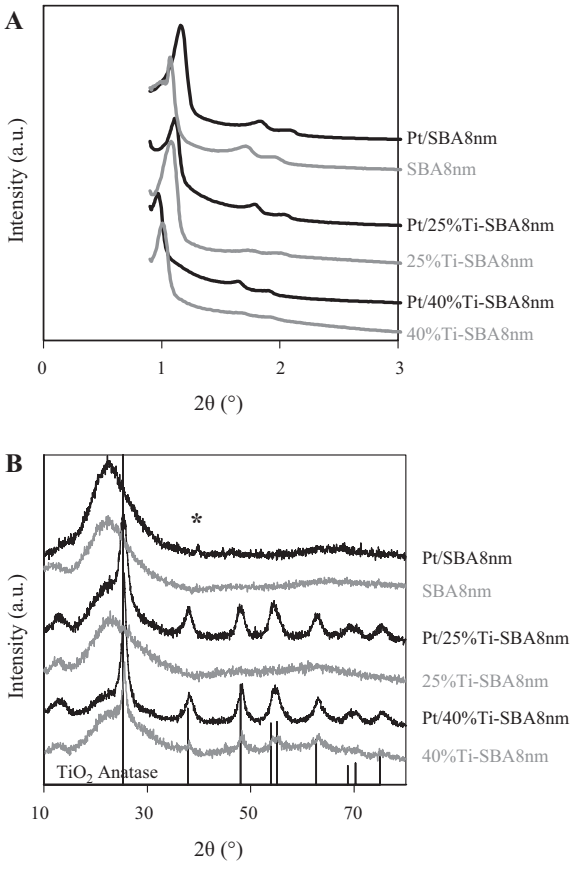

Fig. 1. Small angle (A) and wide angle (B) X-ray diffraction patterns obtained on the Ti-SBA8 nm supports and respective Pt/Ti-SBA8 nm catalysts. (*) Platinum phase detected.

3.1.2. N_2 sorption

The nitrogen sorption isotherms of *x*%Ti/SBA-15 materials and the derived reduced Pt-based catalysts are presented in Fig. 3. The average pore diameters D_p, determined applying the NLDFT theory to the desorption branch of the isotherm, are summarized in

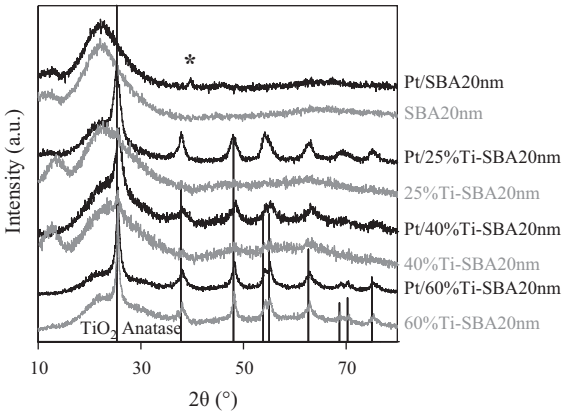

Fig. 2. Wide angle X-ray diffraction patterns obtained over the Ti-SBA20 nm supports and respective Pt/Ti-SBA20 nm catalysts. (*) Platinum phase detected.

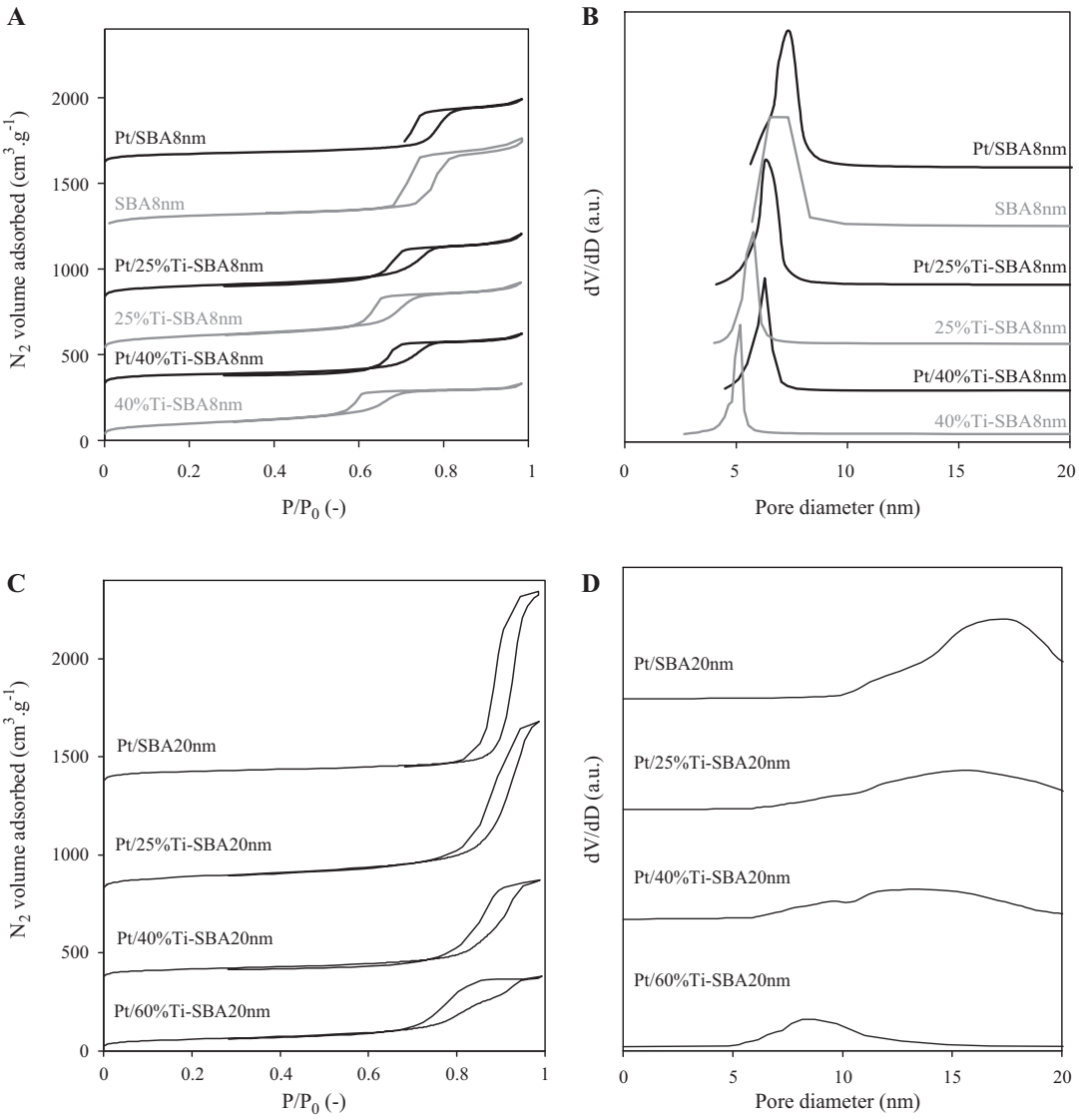

Fig. 3. N_2 adsorption–desorption curves (A and C) and corresponding NLDFT pore size distribution (B and D) obtained over the Ti-SBA8 nm and Ti-SBA20 nm nanocomposites and respective Pt-based catalysts.

Table 1, and the corresponding pore size distributions plotted in Fig. 3. Pore volume and surface area values of the Pt catalysts are also given in Table 1. First, the impregnation of ~1.5 wt.% platinum does not significantly influence the textural properties of the materials, probably due to its low content and the small Pt particle sizes generated. As observed in Table 1, all the Pt/Ti-SBA catalysts display high specific surface areas ($279 \leq S_{BET} \leq 390\ m^2\ g^{-1}$) and mesopore volumes ($0.48 \leq V_p \leq 1.06\ cm^3\ g^{-1}$) compared to the Pt/TiO_2 P25 reference sample ($S_{BET} = 49\ m^2\ g^{-1}$). During the synthesis of SBA support, the addition of hexane allows increasing the pore diameter (D_p) and mesopore volume, leading to large pore SBA-15 materials as expected [33]. This increase can be explained by an increase in hydrophobic micelle volume by incorporation of the swelling agent, resulting in larger pore size in the final material. Nevertheless, the isotherms shape obtained for the two SBA-15 supports (8 nm and 20 nm), as obtained for the derived Pt-catalysts, is of type IV according to the IUPAC classification, which is consistent with the formation of organized mesoporous materials [34,35].

For each catalyst series (from SBA8 nm and SBA20 nm support), the increase in TiO_2 loading leads to progressive decrease of the average pore size, pore volume and surface area (Table 1). The shift of the pore size to lower pore diameters as TiO_2 loading increases is clearly observed in Fig. 3B and D. All materials however present the same type IV isotherms, similar to that of SBA-15 silica (Fig. 3). However, hysteresis loops are slowly shifting from H1 (associated with a narrow pore size and regular cylindrical mesopores) to hysteresis characteristic of pores having constriction [36]. These results are consistent with previous observation, where it was observed that TiO_2 deposition occurs homogeneously and that a TiO_2 film is probably initially formed on part of the internal walls of the mesoporous solid, held at the surface by Si–O–Ti bonds [12]. Nevertheless, thermal treatment at 400 °C leads to the formation of small titania clusters homogeneously dispersed in the SBA-15 tubular pores. Recently, Landau et al. [37,38] studied the insertion of TiO_2 and other oxides in SBA-15 for loadings in the 20–80 wt.% range. Titania is also found as small nanocrystals of 4.5–5 nm, slightly lower than the SBA-15 pore diameter, or as larger crystals with around the same diameter of the used SBA-15 (8.5 nm). The XRD results obtained in this work showed that the crystal size obtained for the anatase phase is in all cases lower than the support pore size, which will lead a limited pore plugging in these materials.

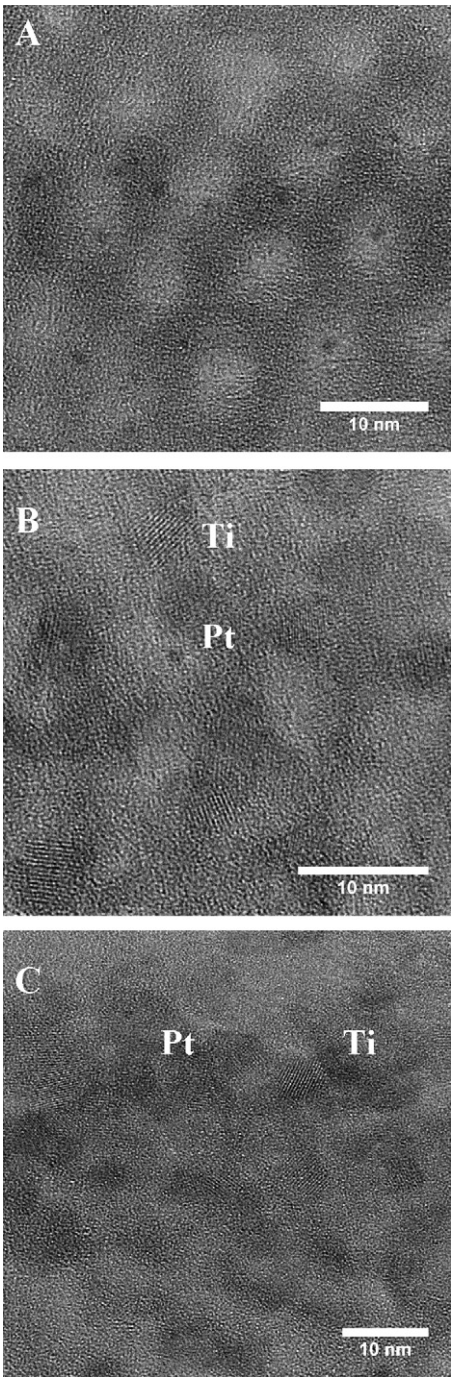

Fig. 4. TEM images of Pt/SBA8 nm (A), Pt/25%Ti-SBA8 nm (B) and Pt/40%Ti-SBA8 nm (C) catalysts.

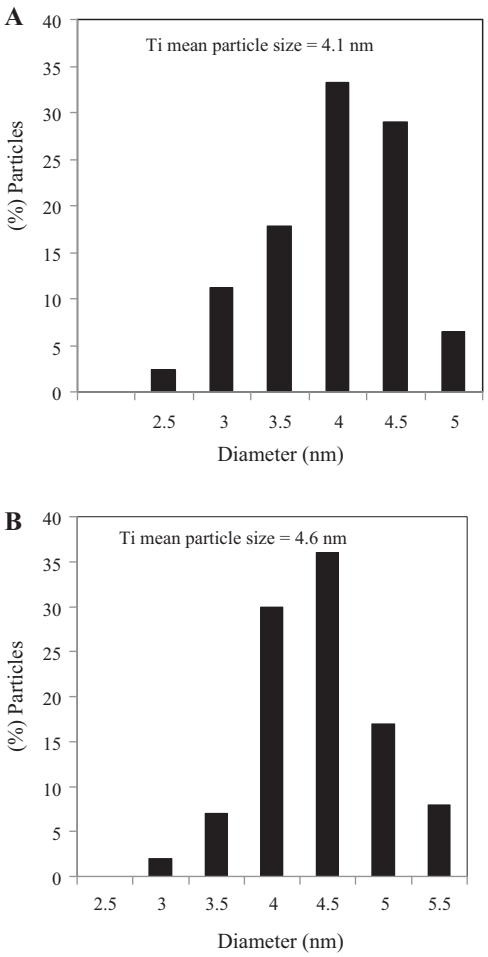

Fig. 5. TiO_2 particle size distributions for Pt/25%Ti-SBA8 nm (A) and Pt/40%Ti-SBA8 nm (B) catalysts.

3.1.3. Transmission electron microscopy

Homogeneity in the distribution of titanium and platinum, and its influence on the well-ordered hexagonal array of mesopores typical of SBA-15, was studied by high resolution transmission electron microscopy (HRTEM), to confirm the results obtained by small and wide angle XRD and N_2-sorption analysis. TEM representative images of the Pt/SBA8 nm, Pt/25%Ti-SBA8 nm and Pt/40%Ti-SBA8 nm catalysts, after reduction at 300 °C, are presented in Fig. 4. As illustrated, pure Pt/SBA8 nm catalyst exhibits a well-defined hexagonal pore structure (Fig. 4A), and the formation of small platinum clusters is clearly observed (dark spots in Fig. 4A). After TiO_2 formation in the pores (Fig. 4B and C), the periodic structure of the SBA-15 framework was always easily observed whatever the TiO_2 content. Crystallized TiO_2 nanoparticles are clearly observed in the SBA pore channels. The Ti and Pt average particle sizes obtained after analysis of characteristic TEM images for all considered samples are summarized in Table 1. The TiO_2 nanoparticle size slightly increases with Ti loading. For example, TiO_2 size histograms presented Fig. 5 show that Ti particle size of the Pt/25%Ti-SBA8 nm catalyst is centered at 4.1 nm, against 4.6 nm for the Pt/40%Ti-SBA8 nm one. The analysis of the TEM micrographs also reveals well-dispersed Pt particles on the support. For all the Pt/Ti-SBA catalysts, the Pt particle sizes are low, with values always comprised between 0.9 and 1.4 nm (Table 1), preventing Pt crystal detection by XRD. Then, the Pt particles seem slightly more dispersed on the Ti-SBA nanocomposites than on TiO_2 P25 and SBA-15 reference supports.

Finally, TEM images obtained for the Pt/25%Ti-SBA20 nm material are presented in Fig. 6. Similar evolutions are observed in materials prepared in this large pore support than in the SBA8 nm support. We can however note that the titania crystal sizes are slightly larger in the SBA20 nm materials than in the SBA8 nm materials (Table 1). Nevertheless, the particle size is largely lower than the pore size of the support, suggesting limited pore plugging. While the XRD did not allowed to conclude on the pore structure (reflection located at too low 2θ to be detected with our instrument), the TEM images suggest a lower structuration quality in these materials, even if the cylindrical pores are always observed in the solids (Fig. 6), even after TiO_2 and Pt^0 particles formation.

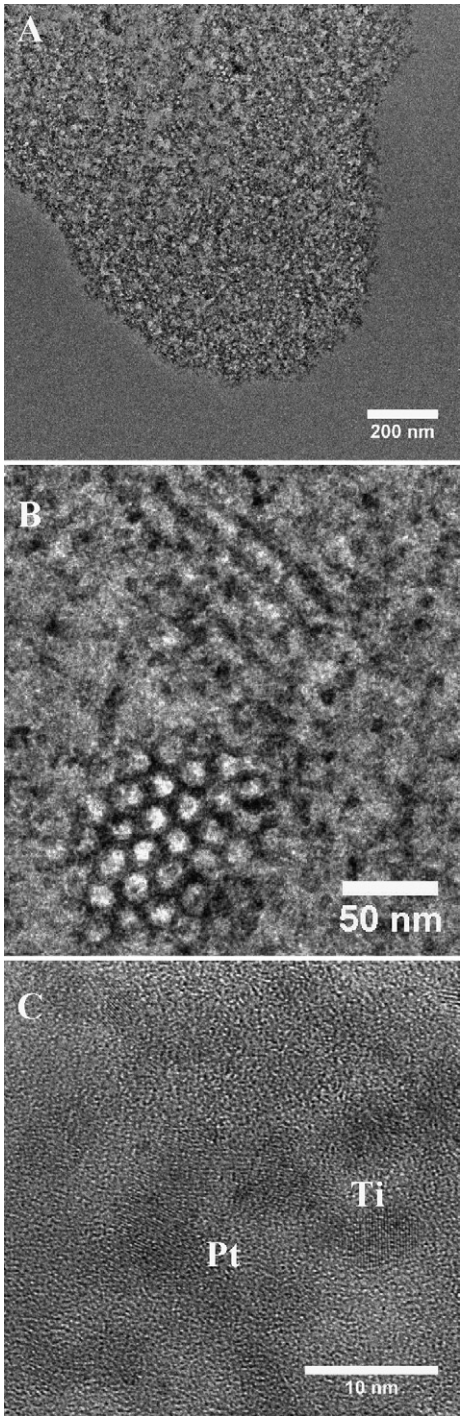

Fig. 6. TEM images obtained for the Pt/25%Ti-SBA20 nm material.

3.2. Citral hydrogenation

Scheme 1 presents the main reaction pathways that can occur during citral hydrogenation. The reduction of citral can lead to a variety of products. A first step is the reduction of either the C=O or the conjugated C=C bond to produce geraniol and nerol (unsaturated alcohols UA), or citronellal, respectively. Consecutive hydrogenation leads to citronellol and finally to 3,7-dimethyloctanol. Apart from these reactions, secondary processes of cyclization or of reaction with the solvent (alcohol) can lead to other by-products like isopulegols or acetals, respectively. Preliminary runs carried out at different stirring conditions, loadings and catalyst grain sizes have demonstrated the absence of external and internal diffusional limitations.

3.2.1. Comparison of the hydrogenating properties of the Pt/TiO_2 P25 and Pt/SBA catalysts

The temporal concentration profiles of the reactant and the main products during citral hydrogenation on the 1.5 wt.% Pt/TiO_2 P25 and 1.5 wt.% Pt/SBA8 nm catalysts are reported in Fig. 7. On the two samples, an important hydrogenation of citral occurs during the first few minutes, with second a rapid deactivation after this earlier period. This behavior is attributed to a decarbonylation reaction of the α,β-unsaturated aldehyde yielding irreversible adsorbed CO that blocked Pt active sites. This phenomenon was already reported by Lercher and co-workers [39,40] during the hydrogenation of crotonaldehyde to crotylalcohol on Pt/SiO_2. On the Pt/TiO_2 P25 sample (Fig. 7A), the main product of citral hydrogenation obtained after 5 min in reaction is citronellal, the formed quantity being progressively transformed further to citronellol, 3,7-dimethyloctanol (listed in "other products") and isopulegol. Beyond 5 min reaction time, citral converts mainly into unsaturated alcohols. This result suggests that the decarbonylation process poisons mainly the C=C hydrogenation sites and modifies the C=C/C=O adsorption competition. In the case of the Pt/SBA8 nm catalyst (Fig. 7B), the temporal profiles are different with citronellal mainly produced even when citral concentration decreases in the reaction medium. Besides citronellal, the products observed in lower quantities are: citronellol ≈ other products (mainly 3,7-dimethyloctanol) ≫ UA > isopulegol. The results clearly show that on SBA-15, the C=C/C=O adsorption competition of the citral molecules is mainly in favor of the C=C bond, leading to a very low UA formation.

3.2.2. Effect of Ti grafting on the hydrogenating properties of the Pt/SBA catalysts

Both 1.5 wt.% Pt/*x*%Ti-SBA (8 and 20 nm) catalyst series were tested for citral hydrogenation under the same experimental conditions (70 °C, 76 bar of hydrogen). Figs. 8 and 9 display the citral conversions as a function of reaction times, and the UA selectivities as a function of citral conversions for each catalyst series. The curves corresponding to the Pt/TiO_2 P25 and Pt/SBA samples are also given for comparison. Figs. 8A and 9A show a decrease of the citral conversion as the Ti loading increases in the Pt/*x*%Ti-SBA catalysts whatever the pore size of the support. Then, the Ti grafting on SBA leads to Pt/Ti-SBA catalysts less active for citral conversion than the Pt/TiO_2 P25 and Pt/SBA samples in spite of the presence of smaller Pt particles on the Ti-SBA nacomposites, and consequently a higher active surface (Table 1). In addition, the same deactivation phenomenon occurs in the first few minutes whatever the pore size of the support and its nature. All these results point out that the pore diameter of the mesostructured SiO_2 is not an influential parameter on the reactivity of the impregnated Pt particles towards citral molecules at these sizes (between 8 nm and 20 nm). Figs. 8B and 9B indicate that the UA selectivity for Pt/SBA (8 and 20 nm) catalysts remains very low whatever the citral conversion (S_{UA} < 6%). As discussed in the previous section, the use of TiO_2 P25 support for Pt impregnation allows improving the selectivity to unsaturated alcohols since S_{UA} can reach 17% at 80% of citral conversion. The TiO_2 dispersion in the SBA8 nm and SBA20 nm supports leads to an improvement of the UA selectivity. The UA selectivity progressively increases with the TiO_2 content for each set reaching values close to 26–28% for the Pt/40%Ti-SBA8 nm and Pt/60%Ti-SBA20 nm at 80% citral conversion. These selectivities are largely higher than those obtained for the Pt/TiO_2 P25 sample. All these results can be explained by the specific role of the reducible TiO_2 species, which can generate a strong metal-support interaction (SMSI effect) with platinum after

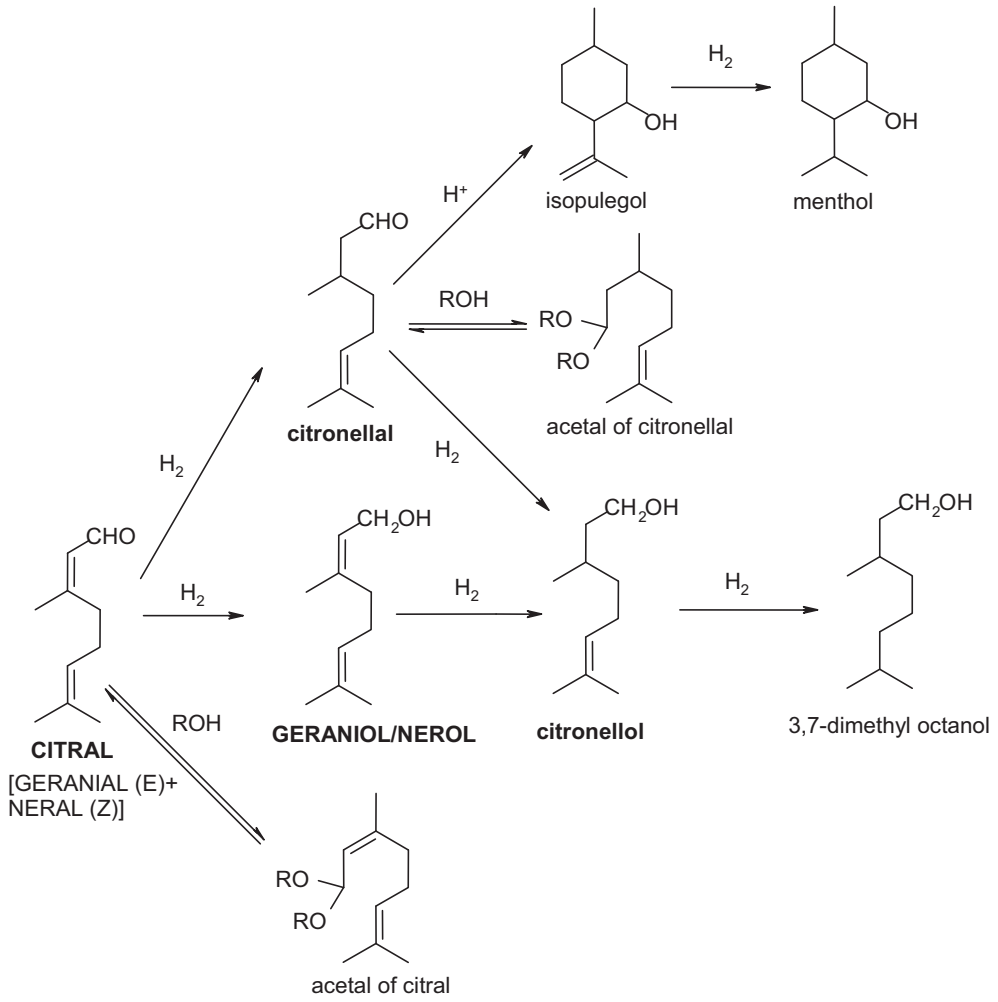

Scheme 1. Reaction scheme for citral hydrogenation.

reduction at 300 °C when anatase nanocrystals are formed [41,42]. The SMSI effect involves the formation of partially reduced $TiO_{(2-x)}$ species ($x < 2$) on the support, which can activate the electronic doublet of oxygen of the carbonyl function and thus can enhance its hydrogenation to the detriment of the conjugated C=C bond [28,29,43]. First, this phenomenon allows explaining the higher UA selectivity obtained on the TiO_2 P25 supported catalyst compared to Pt/SBA samples. Recently, we evidenced that for cyclohexane dehydrogenation, a structure insensitive reaction, the crystal size and crystalline form of titania are two important parameters con-

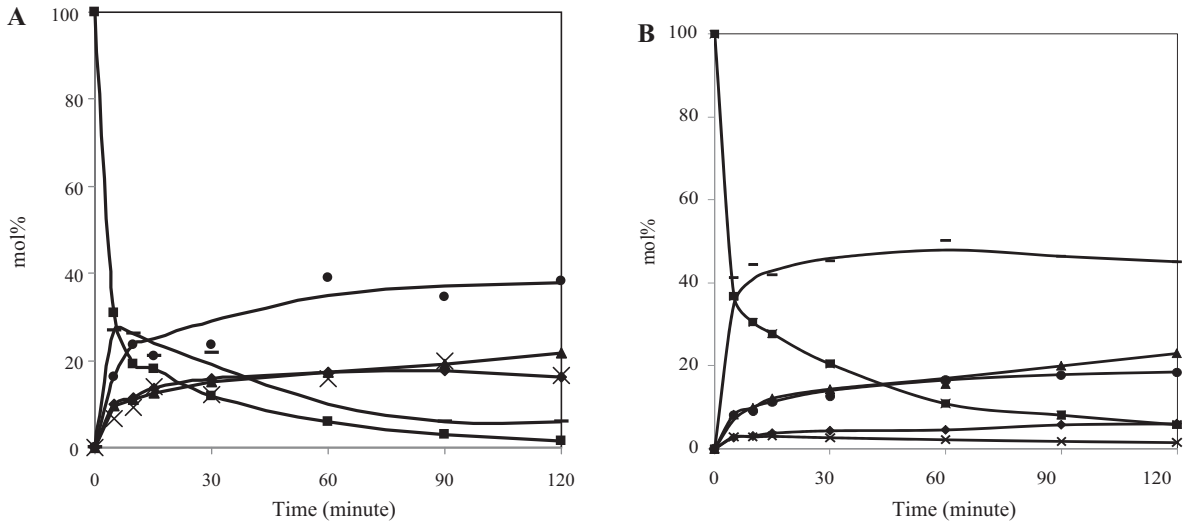

Fig. 7. Hydrogenation of citral on Pt/TiO_2 P25 (A) and Pt/SBA8 nm (B) catalysts: citral (■); citronellal (–); citronellol (▲); unsaturated alcohol (♦); isopulegol (×); others products (●).

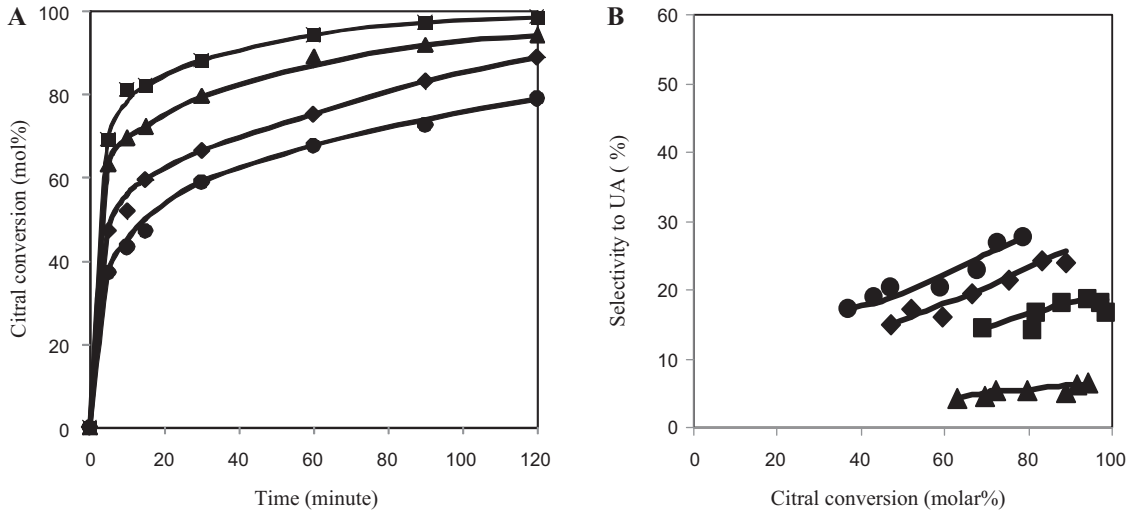

Fig. 8. Citral conversion as function of time (A) and selectivity to unsaturated alcohols (UA) as function of citral conversion (B) over the nanocomposites catalysts: Pt/TiO_2 P25 (■); Pt/SBA8 nm (▲); Pt/25%Ti-SBA8 nm (♦); Pt/40%Ti-SBA8 nm (●).

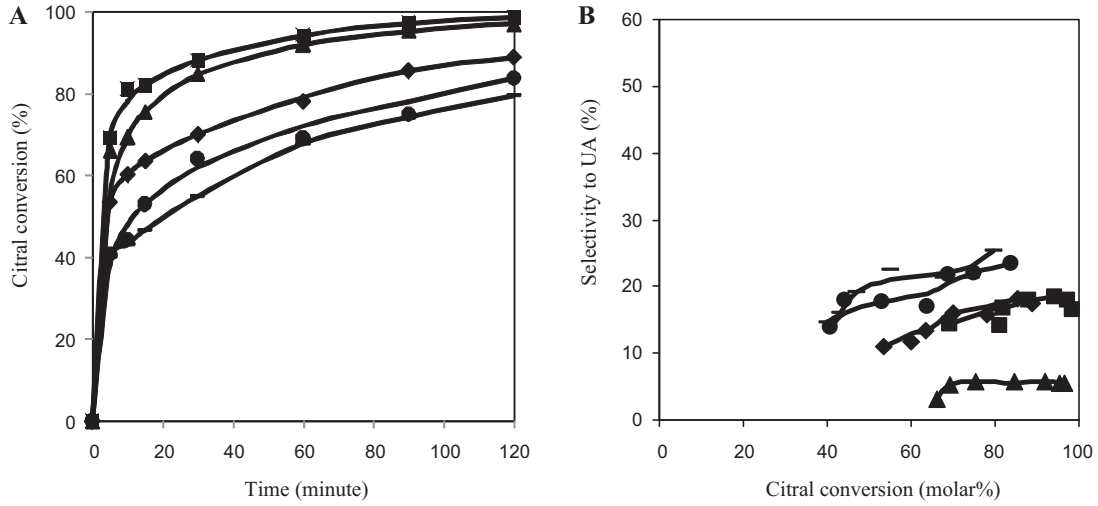

Fig. 9. Citral conversion as function of time (A) and selectivity to unsaturated alcohols (UA) as function of citral conversion (B) over the nanocomposites catalysts: Pt/TiO_2 P25 (■); Pt/SBA20 nm (▲); Pt/25%Ti-SBA20 nm (♦); Pt/40%Ti-SBA20 nm (●); Pt/60%Ti-SBA20 nm (–).

trolling the SMSI effect [41]: (i) for a given crystalline form (for example anatase), the lower the crystal size, the stronger the metal-support interaction; (ii) a lower reduction temperature (<300 °C) is required for anatase titania derived materials to exhibit a SMSI effect compared to that necessary for rutile titania ones. The results obtained in the present study are in agreement with our previous conclusions. Indeed, the grafting of Ti species in the silica porosity is a preparation route allowing the formation of well dispersed anatase TiO_2 nanoparticles [41], which also exhibits improved oxygen mobility [12]. In these conditions, the Pt particles anchored in a well dispersed way on the surface of the Ti-SBA materials should generate Pt atoms–$TiO_{(2-x)}$ species interactions which cover a more important fraction of the metallic active surface than in the case of the TiO_2 P25 support. Logically, lower citral conversions (related to the higher Pt atoms covering) are obtained on the Pt/Ti-SBA catalysts compared to Pt/TiO_2 P25. The increase in TiO_2 content in the composite contributes to emphasize this phenomenon leading to a progressive decrease of the citral conversion, while the UA selectivity progressively increases. Similar conclusions were proposed recently by Rojas et al. during citral hydrogenation over Ir supported on mixed oxides TiO_2/SiO_2 catalysts [44].

4. Conclusion

In this study, Pt catalysts prepared on TiO_2 doped SBA-15 were prepared and characterized. Two mesoporous Pt/Ti-SBA catalyst series were synthesized with 8 nm and 20 nm initial pore diameter, at various titanium loadings. The pore size was increased from 8 to 20 nm by adding hexane as swelling agent before formation of the silica pore structure. The XRD patterns and TEM analysis of the obtained Pt/Ti-SBA materials revealed that the hexagonal mesoporous structure was preserved even after the introduction of Pt or/and TiO_2 in the SBA porosity. Titania and platinum are all in the form of nanoparticles homogeneously dispersed in the silica pore structure. Interesting performances for the selective citral hydrogenation towards unsaturated aldehydes are obtained over these original materials. Compared to a Pt catalyst supported on bulk TiO_2 P25 support, the Pt/Ti-SBA catalysts present lower citral conversions, but higher unsaturated alcohol selectivities which increase with the titanium loading. The results can be explained by an increased interaction between Pt and $TiO_{(2-x)}$ species (SMSI effect) inside the Pt/Ti-SBA nanocomposites, due to the limited size of the anatase titania clusters generated in the porosity. The higher reactivity of these titania nanoparticles is suggested to result in

higher coverage of Pt active surface, which can obviously lead to an increase of the activation of the citral carbonyl function.

Acknowledgements

The AUF (Agence Universitaire de la Francophonie) is gratefully acknowledged for the financial support of this work through a 10 month research grant (T. Ekou).

References

[1] J.S. Beck, J.C. Vartuli, W.J. Roth, M.E. Leonowicz, C.T. Kresge, K.D. Schmitt, C.T.W. Chu, D.H. Olson, E.W. Sheppard, S.B. McCullen, J.B. Higgins, J.L. Schlenker, J. Am. Chem. Soc. 114 (1992) 10834.
[2] D. Zhao, J. Feng, Q. Huo, N. Melosh, G.H. Fredrickson, B.F. Chmelka, G.D. Stucky, Science 279 (1998) 548.
[3] A. Wingen, F. Kleitz, F. SchÜth, Springer Ser. Chem. Phys. 75 (2004) 283.
[4] D.E. De Vos, M. Dams, B.F. Sels, P.A. Jacobs, Chem. Rev. 102 (2002) 3615.
[5] Y. Tang, S. Miao, B.H. Shanks, X. Zheng, Appl. Catal. A 375 (2010) 310.
[6] L.A. Cano, M.V. Cagnoli, N.A. Fellenz, J.F. Bengoa, N.G. Gallegos, A.M. Alvarez, S.G. Marchetti, Appl. Catal. A 379 (2010) 105.
[7] A. Corma, Chem. Rev. 97 (1997) 2373.
[8] S. Damyanova, L. Dimitrov, R. Mariscal, J.L.G. Fierro, L. Petrov, I. Sobrado, Appl. Catal. A 256 (2003) 183.
[9] C. Anderson, A.J. Bard, J. Phys. Chem. 99 (1999) 9882.
[10] H. Chun, W. Yizhong, T. Hongxiao, Appl. Catal. B 30 (2001) 277.
[11] M. Bonne, S. Pronier, F. Can, X. Courtois, S. Valange, J.M. Tatibouët, S. Royer, P. Marécot, D. Duprez, Solid State Sci. 12 (2010) 1002.
[12] M. Bonne, S. Pronier, Y. Batonneau, F. Can, X. Courtois, S. Royer, P. Marécot, D. Duprez, J. Mater. Chem. 20 (2010) 9205.
[13] A. Ungureanu, B. Drăgoi, A. Chirieac, C. Catrinescu, E. Dumitriu, Environ. Eng. Manage. J. 7 (2008) 255.
[14] D. Fattakhova-Rohlfing, J.M. Szeifert, Q. Yu, V. Kalousek, J. Rathouskỳ, T. Bein, Chem. Mater. 21 (2009) 2410.
[15] S.J. Tauster, S.C. Fung, R.L. Garten, J. Am. Chem. Soc. 100 (1978) 170.
[16] R. Vanselow, D. Mundschau, J. Catal. 103 (1987) 426.
[17] M.A. Vannice, B. Sen, J. Catal. 115 (1989) 65.
[18] U.K. Singh, M.A. Vannice, Stud. Surf. Sci. Catal. 130 (2000) 497.
[19] R. Malathi, R.P. Viswanath, Appl. Catal. A 208 (2001) 323.
[20] J. Santos, J. Phillips, J.A. Dumesic, J. Catal. 81 (1983) 147.
[21] G.B. Raupp, J.A. Dumesic, J. Catal. 95 (1985) 587.
[22] P. Chou, M.A. Vannice, J. Catal. 104 (1987) 1.
[23] J.M. Herrmann, M.G.R. Maillot, P.C. Gravelle, J. Catal. 104 (1987) 136.
[24] M.K.I. Senevirathna, P.K.D.D.P. Pitigala, K. Tennakone, Sol. Energy Mater. Sol. Cells 90 (2006) 2918.
[25] C.H. Lin, J.H. Chao, C.H. Liu, J.C. Chang, F.C. Wang, Langmuir 24 (2008) 9907.
[26] P. Panagiotopoulou, D.I. Kondarides, J. Catal. 267 (2009) 57.
[27] J.S. Ratliff, S.A. Tenney, X. Hu, S.F. Conner, S. Ma, D.A. Chen, Langmuir 25 (2009) 216.
[28] T. Ekou, A. Vicente, G. Lafaye, C. Especel, P. Marécot, Appl. Catal. A 314 (2006) 64.
[29] T. Ekou, A. Vicente, G. Lafaye, C. Especel, P. Marécot, Appl. Catal. A 314 (2006) 73.
[30] M. Kruk, L. Cao, Langmuir 23 (2007) 7247.
[31] D.Y. Zhao, Q.S. Huo, J.L. Feng, B.F. Chmelka, G.D. Stucky, J. Am. Chem. Soc. 120 (1998) 6024.
[32] Z. Luan, L. Kevan, Microporous Mesoporous Mater. 44–45 (2001) 337.
[33] M. Kruk, M. Jaroniec, Chem. Mater. 12 (2000) 1961.
[34] M. Kruk, M. Jaroniec, C.H. Ko, R. Ryoo, Chem. Mater. 12 (2000) 1961.
[35] W. Zhang, B. Glomski, T.R. Pauly, T.J. Pinnavaia, Chem. Commun. 12 (1999) 1803.
[36] M.R. Buchmeiser, Polymeric Materials in Organic Synthesis and Catalysis, WILEY-VCH, 2003, pp. 18–20.
[37] M.V. Landau, L. Vradman, A. Wolfson, P.M. Rao, M. Herskowitz, C. R. Chim. 8 (2005) 679.
[38] M.V. Landau, L. Vradman, X. Wang, L. Titelman, Microporous Mesoporous Mater. 78 (2005) 117.
[39] M. Englisch, V.S. Ranade, J.A. Lercher, Appl. Catal. A 163 (1997) 111.
[40] U.K. Singh, M.A. Vannice, J. Catal. 191 (2000) 165.
[41] M. Bonne, P. Samoila, T. Ekou, C. Especel, F. Epron, P. Marécot, S. Royer, D. Duprez, Catal. Commun. 12 (2010) 86.
[42] Y. Li, B. Xu, Y. Fan, N. Feng, A. Qiu, J.M.J. He, H. Yang, Y. Chen, J. Mol. Catal. A 216 (2004) 107.
[43] A.B. Da Silva, E. Jordão, M.D.J. Mendes, P. Fouilloux, Appl. Catal. A 148 (1997) 253.
[44] H. Rojas, G. Borda, P. Reyes, J.J. Martínez, J. Valencia, J.L.G. Fierro, Catal. Today 133–135 (2008) 699.